Electronic Detection of Apoptotic Cells on a Microchip

A K M Arifuzzman [a], Norh Asmare [a], Tevhide Ozkaya-Ahmadov [a], Aref Valipour [a], A. Fatih Sarioglu [a, b, c, *]

[a] School of Electrical and Computer Engineering, Georgia Institute of Technology, Atlanta, GA, 30332, USA
[b] Parker H. Petit Institute for Bioengineering and Bioscience, Georgia Institute of Technology, Atlanta, GA, 30332, USA
[c] Institute for Electronics and Nanotechnology, Georgia Institute of Technology, Atlanta, GA, 30332, USA

[*] Correspondence should be addressed to A.F.S. (sarioglu@gatech.edu)

ABSTRACT

Robust and rapid detection of apoptosis in cells is crucially needed for diagnostics, drug discovery, studying pathogenic mechanisms and tracking patient response to medical interventions and treatments. Traditionally, the methods employed to detect apoptosis rely on complex instrumentation like flow cytometers and fluorescence microscopes, which are both expensive and complex-to-operate except in centralized laboratories with trained labor. In this work, we introduce a microfluidic device that can screen cells in a suspension for apoptosis markers and report the assays results as electronic data. Specifically, our device identifies apoptotic cells by detecting externalized phosphatidylserine on a cell membrane – a well-established biomarker that is also targeted by fluorophore-based labeling in conventional assays. In our device, apoptotic cells are discriminated from others through biochemical capture followed by transduction of individual capture events into electrical signals via integrated electrical sensors. The developed technology was tested on simulated samples containing controlled amounts of cells with artificially-induced apoptosis and validated by benchmarking against conventional flow cytometry. Combining sample manipulation and electronic detection on a disposable microfluidic chip, our cell apoptosis assay is amenable to be implemented in a variety of settings and therefore has the potential to create new opportunities for cell-based diagnostics and therapeutics and contribute to healthcare outcomes on a large scale.

Keywords: apoptosis sensor, cell death detection, Annexin V assay, phosphatidylserine externalization, electronic cell viability assay, microchip-based apoptosis test.

1. INTRODUCTION

Cell death is a fundamental, multi-step process that has profound effect on the function of multicellular organisms and occurs in nominal physiological states in addition to pathological conditions (Galluzzi et al., 2018; Kopeina & Zhivotovsky, 2022). Apoptosis is one of the most

widely recognized and studied type of cell death. The process is controlled and regulated by specific physiological signals or pathological factors (Taylor et al., 2008), allowing detailed study of its mechanics. Necrosis, in contrast, is an uncontrolled cell death typically characterized by cell swelling, followed by membrane rupture and release of intracellular contents (D'Arcy, 2019).

A crucial event that occurs during apoptosis is the externalization of the phospholipid phosphatidylserine (PS), where PS is translocated from its normal inner leaflet placement on the cell membrane to the outer leaflet leaving it exposed to extracellular environment (Balasubramanian et al., 2007). This externalization process is an intrinsic component of tissue regeneration as it marks the cell with an "eat me" signal for neighboring cells and phagocytes whose function is the removal of apoptotic cells. Notably, PS externalization is one of the earlier events in apoptosis, preceding the failure of cell membrane integrity (Kerr et al., 1972). Given the point at which PS externalization occurs relative to the rest of the apoptotic process, detecting externalized PS with a high affinity biochemical probe like Annexin V makes such an assay crucial in studying apoptosis (Meers & Mealy, 1993).

When studying diverse cell populations that are undergoing apoptosis, itself an inherently stochastic process (Darzynkiewicz et al., 2004), it becomes crucial to leverage high-throughput platforms that can perform single cell interrogations. The gold standard for detecting apoptosis is through labeling cells under test with fluorophore-conjugated Annexin V and measuring fluorescence emission with a flow cytometer (Fischer et al., 2002; Vermes et al., n.d.; Worsley et al., 2022). However, this approach is limited in providing immediate interrogations to detect early apoptotic cells as the fluorescence staining procedures require a lead time before the sample is ready for analysis (Schutte et al., 1998). Moreover, fluorescence labeling has the potential to compromise protein activity due to the chemical cross-linking reactions present during the staining process (Koskinen et al., 2004). In addition, a flow cytometer is a complex instrument with a large footprint. Due to high maintenance costs and operational complexities, flow cytometers are often deployed in shared facilities and operated by skilled technicians, making it impractical to perform apoptosis assays at the point-of-care (PoC) or in mobile testing environments. Additionally, the extensive number of operational parameters that need to be manually selected, along with the necessary sample preparation, make the entire process and the interpretation of results dependent on the specific operator or laboratory conducting the analysis.

Several studies have leveraged recent technological advancements to develop apoptosis detection techniques, with the most common approaches utilizing fluorescence microscopy and image-based cytometry. One such study utilized a novel tetrahedral DNA probe to simultaneously image intracellular cytochrome c and telomerase to provide a comprehensive visualization of the apoptotic process (Dong et al., 2022). Another approach developed a microfluidic multicellular coculture array to integrate multiple cell-based assays, one of which was apoptosis detection, into a unified system (Chong et al., 2022). Alternatively, several electrochemical approaches have also emerged, including an Annexin V-modified biosensor that uses an impedance spectroscopy scheme to identify early apoptotic cells (Tong et al., 2009) and a differential pulse voltammetry (DPV) based measurement of caspase-3 activity that is used as an indicator of

apoptotic activity (Chen et al., 2015). All these sensing methods, however, suffer from low portability and/or high cost due to their instrumentational and operational complexity.

In pursuit of assays that are more portable and affordable than conventional assays, significant advancements have been made using microfluidic microchip-based technologies. These solutions typically feature sensing elements integrated on-chip to allow compact sensing while maintaining direct contact with the cell sample (Arifuzzman et al., 2023; Civelekoglu et al., 2019; Civelekoglu, et al., 2022; Civelekoglu, et al., 2022; Civelekoglu, et al., 2022; Liu et al., 2019, 2020). These studies, however, adopt an immunoanalytical approach to target surface markers and do not directly target apoptotic cells.

Here, we introduce a microchip-based apoptosis assay that detects apoptosis by targeting externalized PS on cell membranes, eliminating the need for the user to pre-label the sample before performing the assay. This is a crucial advantage, since traditional testing practices such as flow cytometry require a multiple, labor-intensive sample preprocessing steps before running the assay. These steps typically include preparing various dilutions of the stock reagent, correctly mixing the diluted label solution with the sample, waiting for incubation, and performing centrifugation and resuspension. In contrast, our microchip-based apoptosis assay significantly simplifies this process by incorporating the sample preprocessing steps—such as labeling and mixing—directly within the microchip itself. This is made possible through our unique microchip design and manufacturing process, which chemically modifies specific regions within the microchip. These modifications allow the necessary chemical reactions to occur automatically when the sample is loaded, without any manual intervention. For the end user, this means that the sample can be directly loaded into the microchip without the need for dilution, mixing, incubation, or centrifugation. The entire process is automated within the microchip, resulting in a rapid, label-free apoptosis assay with a streamlined workflow. This not only reduces the time and effort required but also minimizes the potential for human error, making the assay more efficient and user-friendly. This capability makes our platform well-suited for integration with automated cell development processes, enabling efficient and flexible apoptosis assays as required. Additionally, the microchip-based assay allows it to be portable for deployment in point-of-care settings unlike a flow cytometer. This is particularly advantageous in remote or resource-limited environments where traditional laboratory facilities are inaccessible, enabling apoptosis assays to be performed efficiently and effectively outside of conventional laboratory settings. To develop an apoptosis assay platform with sample-to-answer capability, cells are internally labeled in flow on our microchip to transduce relatively weaker Annexin V-PS affinity into stronger avidin-biotin binding for reliable biochemical capture of apoptotic cells. A network of barcoded electrical sensors then quantifies the fraction of cells with externalized PS expression through capture statistics and presents the data as an electrical output signal. We applied our assay on studying human t-cell lymphocytes subjected to heat to induce apoptosis and validated it accuracy by benchmarking against the well-established flow cytometry-based Annexin V assay.

2. MATERIAL AND METHODS

2.1. Chemicals and materials

We acquired the materials and chemicals used in this work from various sources. 3-aminopropyltriethoxysilane (APTES) was purchased from Gelest, Inc., while Neutravidin and BSA (Bovine Serum Albumin) were obtained from Thermo Scientific. Glutaraldehyde and trichloro(octyl)silane were sourced from Sigma-Aldrich, and 200 proof ethanol was obtained from Decon Labs, Inc. Phosphate-Buffered Saline (PBS) was purchased from Mediatech, and all chemicals used were of analytical grade. The experiment also utilized deionized (DI) water.

The FITC Annexin V (Cat. No. 640906), Biotin Annexin V (Cat. No. 640939), and Annexin V Binding Buffer (Cat. No. 422201) were sourced from BioLegend (San Diego, CA). Cy5 biotin conjugate (Cat. No. 3100) was purchased from AAT Bioquest, Inc. (Pleasanton, CA). The Jurkat Clone E61 (ATCC® TIB152™) cell line was procured from the American Type Culture Collection (ATCC) (Manassas, VA). The Roswell Park Memorial Institute Medium (RPMI 1640), fetal bovine serum (FBS), and 1% Penicillin/Streptomycin antibiotics were all acquired from Corning (Corning, NY).

For materials used during fabrication, 4-inch diameter silicon wafers were procured from UniversityWafer, Inc. SU-8 2000 series photoresist was obtained from MicroChem, while NR9-1500PY negative photoresist was acquired from Futurrex, Inc. Lastly, polydimethylsiloxane (PDMS) elastomer Sylgard 184 was purchased from Dow Corning.

2.2. Microchip fabrication

The microchip was fabricated using soft lithography and surface micromachining techniques. First, a 15 μm thick layer of negative photoresist SU-8 (SU-8 2025, MicroChem) was spin-coated onto a silicon wafer. The design micropattern was transferred to the photoresist film by exposing it using a maskless aligner (MLA-1500, Heidelberg). The photoresist was then developed with a SU-8 developer (SU-8 Developer, MicroChem) to create the negative mold. The micropatterned wafer was then treated with trichloro(octyl)silane in a desiccator for 8 hours before a mixture of PDMS elastomer and its crosslinker (Sylgard 184 kit, Dow Corning) was prepared at a 10:1 weight ratio. This polymer mixture was poured onto the mold, degassed, and cured at 65 °C for 4 hours. The resulting PDMS was then peeled off and cut into individual chips.

To fabricate the electrical sensor network, a 1.5 μm thick layer of negative photoresist (NR9-1500PY, Futurrex) was spin-coated onto a 2-inch by 3-inch glass microscope slide (6101, Premiere). Then, the microelectrode pattern was transferred to the resist layer using a maskless aligner (MLA-1500, Heidelberg). The photoresist layer was then developed using a developer (RD6 developer, Futurrex). To prepare the glass slides for the subsequent deposition process, a reactive ion etcher was used for descumming, ensuring optimal surface conditions. Using an electron beam evaporator, a 20 nm-thick chromium (Cr) film was deposited onto the glass slides, followed by the deposition of a 250 nm-thick (Au) film. This process ensured the formation of a reliable metal stack with strong adhesion to the glass surface. The sacrificial photoresist layer

was removed by submerging the glass substrate in an acetone bath while employing mild sonication. Finally, the PDMS layer and the glass substrate were subjected to a one-minute oxygen plasma treatment to activate their surfaces. The activated PDMS layer and the treated glass substrate were aligned under a microscope and bonded together at a temperature of 65 °C to form the final structure.

2.3. Measurement of micromixing efficiency for on-chip cell labeling

Dye solutions with different colors (red and blue) were used in lieu of actual samples and reagents to evaluate different on-chip mixing strategies. Then, to quantify the efficiency of a specific microchip design, we calculated a mixing index (MI), which was derived based on the levels of primary color components within a 30 μm by 30 μm region of interest (ROI) in acquired images (São Pedro et al., 2023). Specifically, by measuring the presence of blue and red color content at distinct points throughout the mixer flow stream, we quantified the extent of mixing at various positions of interest. For each ROI, this measurement is done by first splitting the image into red, green and blue color channels. Omitting the green channel, the red and blue color channels of the ROI image are both converted into 8-bit grayscale, i.e., the intensity value of each pixel was converted into 8-bit levels–where 0 represents completely black and 255 represents the highest color intensity. Splitting and normalizing the individual color channels this way allows the use of their intensity values in direct comparative analysis. Then, we determined the MI by computing the intensities of red and blue color channels within the ROI, at a given point on the mixer, relative to the intensities of red and blue color channels of the red and blue dyes before they enter the mixer. This normalization was deemed necessary as the stock red and blue dyes did not exhibit the same intensity values when converted to grayscale. Hence, assuming a value of 255 for both the red color channel intensity of the red dye and blue color channel intensity of the blue dye would lead to erroneous calculations. All in all, we calculated the MI as:

$$\mathrm{MI} = 100\,\% - \left(\frac{\left|(R_{ROI} - B_{ROI)}\right| - \left|(R_{unmix} - B_{unmix)}\right|}{R_{unmix}} \times 100\,\%\right)$$

,where R_{ROI} and B_{ROI} represents the amount of red and blue dye content measured in the ROI, respectively. R_{unmix} and B_{unmix} denote the red and blue channel intensities measured at the red and blue dye inputs of the mixer, which were used to normalize the measured red and blue channel intensities at the various points throughout the mixer.

2.4. Chemical functionalization of the microchip for apoptotic cell capture

We chemically functionalized inner surfaces of our fabricated microfluidic device to selectively capture the target cells out of a heterogenous mix. To utilize plasma-assisted surface activation for the subsequent chemical treatment, the process was initiated within the first 10 minutes after oxygen plasma-assisted PDMS-glass microchip bonding was performed. All chemical reagent infusions, including the washing step, were conducted at a flow rate of 500 μL/hr, with each infusion having a duration of 20 minutes. First, the device was wetted with ethanol followed by flushing the device with a solution of APTES in ethanol (3% v/v). Following an incubation of 1 hour, the device was washed with ethanol and dried in a vacuum oven at 110 °C for 1 hour. The

device was then washed with deionized (DI) water, infused with a glutaraldehyde solution in DI water (3% v/v) and incubated at room temperature for 1 hour. We measured the cell speed in the microfluidic channel to ensure that the presence of glutaraldehyde within the microchip does not significantly affect it (Fig. S1 and Supplementary Video 1). Our findings indicate that the glutaraldehyde treatment does not impact the fluidity of the infused sample during operation when compared to an identical microchip without glutaraldehyde treatment. To continue the surface modification process after glutaraldehyde treatment, the device was flushed with DI water and then infused with a 1 mg/mL neutravidin solution in PBS. A total of 166.7 µg of neutravidin was infused over a 20-minute period at a flow rate of 500 µL/hr. Following this, the device was incubated for 4 hours at room temperature to facilitate glutaraldehyde-neutravidin binding and then flushed with PBS. To confirm consistent neutravidin immobilization, we conducted a characterization experiment. Three identical neutravidin-functionalized microchips were prepared alongside one control device without neutravidin. All four devices were incubated with Cy5-biotin for 1 hour, washed with PBS, and examined using fluorescence microscopy to measure fluorescence intensity. Cy5-biotin was selected because its presence after the labeling and washing steps indicates the presence of neutravidin, which would be absent if neutravidin had not been immobilized on the microfluidic walls and pillars. Fluorescence intensity was measured at three different locations on each device, and the average fluorescence intensity across the three neutravidin-functionalized devices was found to be similar (Fig. S2). This confirmed the consistent immobilization of neutravidin across different devices using our chemical immobilization process. Next, the device was flushed with PBS and incubated with a 3% BSA blocking buffer for 1 hour for blocking the surface against non-specific cell capture. Finally, the device was thoroughly washed with PBS to remove unbound neutravidin, completing the functionalization process and producing a microchip ready for processing a sample.

2.5. Preparation of human T lymphocyte samples

Immortal T lymphocyte cells (Jurkat, Clone E6-1-TIB-152) were acquired from the American Type Culture Collection. After thawing, cells were cultured in RPMI media, supplemented with 10% FBS and 1% Penicillin antibiotics to support optimal growth. The cells were cultured in media in a T25 flask within an incubator that was maintained at 37 °C and 5% CO_2. Once the cells reach a confluency of 80%, they were collected and resuspended in 1X PBS before being placed in vial for use in experiments.

2.6. Induction of controlled apoptosis on samples

Jurkat cells were artificially induced into apoptosis using heat shock. Heat-induced apoptosis is a commonly observed phenomenon in heat-related illnesses, where irreversible cellular damage occurs at elevated temperatures ranging from 46 °C to 60 °C (Leber et al., 2012). In this work, Jurkat cells were exposed to 70 °C for 15 minutes to trigger the apoptotic processes. Following the heat exposure, the cells were immediately resuspended in fresh medium (RPMI 1640, Corning) and placed in a 5% CO_2 incubator set at 37 °C to maintain them in a stable environment for further analysis. Cells were then sampled for analysis at different time points over a 12-hour period as they underwent apoptosis. Sampled cells were suspended in an Annexin V binding buffer solution containing Ca^{2+} ions to facilitate Annexin V-PS binding.

2.7. Experimental setup

The cell suspension and biotin-conjugated Annexin V solution were each loaded into separate 1 mL syringes and infused into the microchip using a syringe pump running at a controlled flow rate of 100 µl/hr. The on-chip electrical sensor network was excited by a 2 Vpp sinusoidal wave at 550 kHz through the input electrode pads. The current waveforms produced at the output pads were first amplified and converted into voltage signals using transimpedance amplifiers (TIA) and then demodulated by the lock-in amplifier (LIA) (HF2LI, Zurich Instruments). The baseband signal stream, time waveform recording of the barcoded sensor activity corresponding to detections of individual cells, was sampled at 57.57 kSa/s into a computer and processed by a custom-built algorithm suite that performed signal pre-processing and analytics.

2.8. Flow cytometry validation

We labeled a sample being validated with FITC Annexin V (BioLegend). To label the sample, cells were first washed twice with PBS and then resuspended in Annexin V binding buffer (BioLegend) at a concentration of $1x10^6$ cells/mL. Next, 100 µL of the cell suspension was transferred to a 5 ml test tube, and 5 µL of FITC Annexin V was added. The cells were gently vortexed and incubated for 15 minutes at room temperature (25 °C) in the dark. Finally, the sample was diluted by adding 400 µL of Annexin V binding buffer (BioLegend) to the tube. Once labeled, the sample was introduced into the flow cytometer (LSR-II, BD Biosciences) and subsequently, the laser power values were configured for optimal measurement (FSC: 275 V, SSC: 250 V, and FITC: 250 V). For every sample being validated, the processing was stopped once 5000 events were recorded. Finally, we analyzed the flow cytometry data using FlowJo (FlowJo, LLC).

3. RESULTS

3.1. Microchip design and assay workflow

We designed our microchip to (1) discriminate between apoptotic and non-apoptotic cells through biochemical capture of those presenting PS on their membrane and (2) convert cell capture statistics to electrical data for the number of apoptotic cells in the sample (Fig. 1a). For the biochemical capture stage, we have determined the Annexin V-PS affinity to be not sufficient to capture cells in a flow stream within our device in contrast to the avidin-biotin affinity, despite the fact that Annexin V is widely used to specifically label externalized PS on apoptotic cells in suspension (Abbady et al., 2017; Vermette et al., 2003) (Fig. S3). As a solution, we aimed to capture apoptotic cells on our device via stronger avidin-biotin binding, which required labeling of cells before they are introduced to the capture chambers. Therefore, we designed our microchip to label apoptotic cells with biotin while they flow within the device and specifically capture the labeled cells on surfaces functionalized with avidin (Fig. 1a). The microchip has two inlets that symmetrically feed a micromixer stage, where one inlet is used to introduce the cell sample to be interrogated while the other is used to introduce a buffer containing biotinylated Annexin V. In the mixer, the cell sample and Annexin V solution are mixed to ensure a

consistent distribution of Annexin V throughout the sample. Next, the mixed solution is delivered to the cell capture chamber functionalized with neutravidin, where the apoptotic cells labeled with biotinylated Annexin V are captured on the micropillars via the strong avidin-biotin interaction and the non-apoptotic cells are let to be discharged from the outlet. For the quantification of assay results, we integrated an electrical sensor network into the microchip, which logs individual cells as they enter and exit the capture chamber. Detected cells generate coded electrical signals, which are first sampled into a computer and are processed. The fraction of cells captured by the chamber are finally computed and scored as apoptotic (Fig. 1a).

The fabricated microchip consisted of two parts: a passive microfluidic layer and an integrated electrical sensor network (Fig. 1b). The microfluidic layer was created by molding PDMS via a standard soft lithography process. The dimensions of microfluidic structures were optimized to work with the target cell population, i.e., human T-cells, which have an average diameter of 11-14 μm. The microfluidic channel was 20 μm high, which allowed unobstructed flow of suspended cells while ensuring cells proximity to the electrical sensors on the channel floor. The capture chamber was designed to be a 145 mm-long 1.5 mm-wide serpentine channel that contained micropillars, which served both to increase the functional surface area and to structurally support ceiling of the wide microchannel against collapse. As expected, a higher density of micropillars was found to enhance the capture efficiency (Fig. S4). To optimize spatial distribution of captured cells, micropillars were arranged in three zones with increasing density. In the first zone, we intentionally maintain a lower pillar density to reduce the risk of cell clogging (Fig. S5), at the cost of a reduced capture rate (< 79%) (Fig. S4). Cell clogging promotes non-specific mechanical immobilization of cells regardless of whether or not they are apoptotic–increasing the false positive detection rate. The second and third zones, in contrast, are designed to progressively favor cell capture efficiency, ultimately achieving > 92%, by maintaining increasing pillar densities (Fig. S4). Since a significant portion of the cell population is captured in the first and second zones, the likelihood of cell clogging in the third zone, which has highly dense micropillars, is significantly reduced. This strategic heterogeneous micropillar design ensures a more effective and reliable cell capture across the entire device. The micropillars of first and second zones were arranged in a grid pattern and had 50 μm lateral spacing. While the first zone kept a 160 μm longitudinal spacing between micropillars, this value was reduced to 50 μm in the second zone for a more densely packed section. The third zone featured a two-position staggered micropillar arrangement, where both lateral and diagonal spacings were 15 μm (Fig. 1c and Fig. S5).

Besides the main fluidic pathway taken by the cells, the microfluidic layer contained auxiliary functionalization ports and channels that were located near the inlet and outlet of the capture chamber. These peripheral channels enabled exclusive delivery of reagents to the target area, ensuring cells to be exclusively captured in intended locations. Built-in particulate filters within these channels prevented coagulate products or precipitation from forming and entering the chamber during the introduction of the different functionalization reagents. The auxiliary ports were sealed following functionalization, leaving the microchip with two inlets and a single outlet.

The second major component of our microchip, the electrical sensor network, comprised of two barcoded sensors strategically positioned before and after the cell capture chamber, enabling a precise count of each cell captured in the chamber (Fig. 1b). We designed the sensor network based on the Microfluidic CODES platform (Liu et al., 2016, 2017), which utilized a code multiplexed architecture that allows spatiotemporal tagging for cells from an electrical signal. The barcoded sensors consisted of positive and negative output electrode fingers, acting as current sinks, while a common input electrode served as the current source. The fingers were arranged in an interdigitated manner such that the common electrode formed pairs with either the positive or negative electrodes at prescribed locations in the sensor. These pair arrangements determined the waveshape produced by the sensor and were hence designed to follow a known and desired sequence. Each sensor consisted of 15 pairs of electrodes (Fig. 1b), resulting in a bipolar waveform with 15 peaks, each representing a bit in the code sequence. The unique waveforms were processed through a correlation-based algorithm that matched each waveform with its corresponding sensor, thereby determining the time and location of the detection event. By aggregating detection events from the entry and exit sensors and using them in a mass balance equation, we determined the number of apoptotic cells captured in the chamber. It should also be noted that the barcoded sensor network was designed to detect cells at multiple locations simultaneously, all from a single electrical output within a single microchip. This eliminated the need for additional external electrical sensing and circuitry for each individual sensor, making it possible to potentially expand the platform to include additional chambers with different chemicals or antibodies without increasing the device complexity. Moreover, our on-chip barcoded sensors are passive, avoiding any additional complexity to the microfluidic device itself and relying on advanced computational algorithms to interpret the electronic measurements.

3.2. On-chip labeling of apoptotic cells

To efficiently discriminate between apoptotic and non-apoptotic cells, we evaluated different capture strategies for our assay. As mentioned previously, biochemical capture of PS-expressing cells via Annexin V immobilized on our microchip resulted in an inefficient capture (~16%) of the target cells (Fig. S3). In contrast, we found that when cells from a matched sample were pre-labeled with biotin, they were captured on an avidin-functionalized device with high (~93%) efficiency. Based on these results, we decided to target apoptotic cells via strong avidin-biotin binding in our assay. However, in order to create an assay that can directly operate on unlabeled samples, we aimed to perform the labeling of the cells within our microchip. In our device, cells were introduced into a biotinylated Annexin V solution before they reach the capture chamber so that biotin-expressing cells can be selectively captured on the avidin-coated micropillars.

To automatically label cells in flow, we built and tested passive micromixers with different geometries (Fig. 2a). Serpentine, triangular and linear mixers, each composed of 50 repeating units (Fig. S6), were tested by measuring their efficiency in mixing dye solutions with different (red and blue) colors when each were simultaneously driven at a flow rate of 100 μL/hr. Processing the microscope images taken at the output of different mixers, we calculated a mixing index (MI) (Materials and methods), which served as a metric that represents the effectiveness of

each micromixer design. From our study, we found the triangular micromixer (MI, 93.9%) to be more efficient than the serpentine (MI, 86.5%) and linear (MI, 34.9%) micromixers and utilized this design in our assay.

Next, we optimized the triangular micromixer design and operating conditions to maximize the mixing efficiency. First, we measured the MI at various stages of the micromixer (Fig. 2b) and concluded that 50 mixing units was sufficient to thoroughly (MI, 94.3%) mix the fluids. Then, we studied the effect of turn angle on the mixing performance. We constructed several triangular micromixers with turn angles ranging from 5° to 20°, each with 50 units, and analyzed them (Fig. 2c). While, we observed the mixing performance increased with the turn angle, i.e., the 5° design produced an MI of ~79.3%, whereas a 20° design produced an MI of ~95.2%, larger turn angles also increased the micromixer footprint. Based on these results, we have settled on channels with 15° turn angle going forward. Finally, we investigated the impact of flow rate on the mixing efficiency (Fig. 2d). We tested a range of flow rates (50-200 μL/hr), which were identical across the two inlets. We found that higher flow rates led to better mixing with the MI increasing from ~70.2% to ~94.8% as the flow increases from 50 μL/hr to 200 μL/hr. Considering the negative impact of higher flow rates on subsequent capture stage and the diminishing returns on mixing efficiency for flow rates >100 μL/hr (Fig. 2d), we decided to operate the micromixer at a flow rate of 100 μL/hr from each inlet.

Lastly, our on-chip labeling process eliminates the need for manual sample labeling, which traditionally involves several complex steps. In contrast, our on-chip micromixer-based apoptosis assay platform significantly simplifies the workflow for the end user. Users simply need to introduce an unlabeled sample, and the microchip autonomously handles the internal labeling necessary for the apoptosis assay. This enables our microchip-based apoptosis assay platform to provide a label-free experience for the user.

3.3.Processing of cell capture signals

To acquire electrical data from the sensor network tracking cells in our microchip, we built a system comprising of both hardware and software components (Fig. 3a). The hardware was responsible for (a) generating a sinusoidal waveform (550 kHz, 2Vpp) for driving the microchip to excite the embedded sensors and (b) collecting the cell detection-bearing signal output by the microchip and conditioning it for sampling. Due to the interdigitated arrangement of the drive and sense electrode fingers in each sensor, the injected sinusoidal waveform creates localized, alternating current electric fields in the volume above each sensor through which cells flow. When doing so, the flowing cells create intermittent changes in these electric fields that is reflected in the electrical current between the electrodes. The raw current (typically 1-10 μA) is first amplified by a low-noise transimpedance amplifier (TIA) with a gain of ≥1000x. The amplified signal is then demodulated within a lock-in amplifier (LIA) to separate the baseband cell signals from the carrier sinusoidal that was initially used to excite the microchip. This demodulated signal appears as a digital stream of barcoded sensor signals; all limited to ≤ 5kHz bandwidth. Next, this cell signal stream is low-pass filtered (f_{3dB} 10kHz) and sampled at 57.57 kSa/s before being saved to computer memory. Regarding the sampling rate, since the cell signals' bandwidth does not exceed 5 kHz, a 20 kS/s rate meets the Nyquist criterion. However, we chose 57 kS/s to provide a spectral buffer. Finally, this sampled data is used in the subsequent

signal processing stages to produce a count of apoptotic and non-apoptotic subpopulations present in the cell sample flowed through the microchip.

We developed a two-stage algorithm to interpret signals extracted from the microchip. The first stage screened the raw signal stream produced by the LIA and identified the time segments that contained sensor activity from cell detection (Fig. 3b). The segmentation was based on a sliding window that ran across the raw signal stream and saved the ones which had a power greater than a threshold. This threshold was set to be 34 dB above the noise floor, which was in turn determined by first aggregating signal windows during the initial 5 seconds of program and device operation. Then, 100 time-windows with the lowest powers were identified and averaged to set the noise floor. Any detection events with power below this threshold, primarily generated by debris, lysed cells, or small particles, were discarded.

The second stage of our algorithm correlated the pre-constructed template library with segmented signals that only contained sensor activity to identify the specific sensor generating the signal. The template library was constructed by first generating digital code signals, i.e., bipolar square waves that each followed the bit sequence encoded in each sensor. Using these digital waveforms for correlation, we first identified 20 low distortion, high SNR (>39 dB) sensor waveforms from the signal stream for each code. All sensor waveforms with the same code were normalized in power and time before being averaged to produce the template for that code. Similarly, any cell signals that could not be matched with any template were eliminated from further analysis. Then, we identified the sensor ID by running cross-correlation between the sensor waveform and each of the templates in the library. The correlating template that had a greater than 80% match was used to determine which sensor detected the event in question (Fig. 3c). This was repeated for all waveforms in the signal stream to aggregate a count of every event detected by each sensor.

In the final stage of signal analysis, the algorithm mapped the aggregated cell events to corresponding sensors on the microchip (Fig. 3d). Namely, since the positions of the sensors and their codes were known, each cell event was used to keep a running tally of the cells detected by each sensor. Once the location of all the cell events had been registered, the algorithm then computed the difference between the total number of cells registered at the entry sensor, which represented all the cells processed by the microchip, and the total number of cells registered at the exit sensor, which represented the uncaptured, non-apoptotic cells. Therefore, the differential count between the two sensors was interpreted as the number of apoptotic cells in the sample under test (Fig. 3d).

3.4. Biochemical capture of apoptotic cells

To ensure reliable cell capture, we optimized the process to chemically functionalize the microchip. We chemically treated the microchip to immobilize neutravidin on the inner surface (Materials and methods) to target the apoptotic cells already bound to biotinylated Annexin V from the micromixing stage. As a first step, we aimed to validate the functionalization process by investigating the neutravidin coating by introducing fluorophore-conjugated biotin in the device followed by imaging with fluorescence microscopy (Fig. 4a). The results confirmed successful immobilization of neutravidin uniformly across the device. It should be noted that, while all

inner surfaces of the microchip were coated with neutravidin, only capture chamber was designed to provide a combination of low flow speed and surface are to promote apoptotic cell capture.

Next, we investigated the cell capture efficiency as a function of biotin-labeling of target cells. For this analysis, we used biotinylated Annexin V solutions with different concentrations (2-10 μg/ml) and measured the total number of apoptotic Jurkat cells captured on the device when matching cell populations were processed (Fig. 4b). We observed an increase in capture with biotinylated Annexin V concentration as increasing the concentration from 2 μg/ml to 10 μg/ml improved the capture efficiency from ~36.6% to ~93.7%. Based on these results, we attributed the poor capture performance at lower concentrations to a shortage of available biotinylated Annexin V molecules to bind to the surfaces of apoptotic cells and set the labeling solution concentration to 10 μg/ml for the remainder of this study.

While the abundance of biotinylated Annexin V ensured efficient on-chip labeling of target cells, excess unbound amount presented a challenge as they bonded with avidin on the device surface competing with the labeled target cells. We aimed to quantify the effect of unbound biotinylated Annexin V on the target cell capture efficiency by monitoring changes in the capture rate with increasing unbound biotinylated Annexin V in the microchip. In our measurements, apoptotic Jurkat cells at a concentration of $4x10^6$ cells/ml were driven through the microchip along with a biotinylated Annexin V solution at a concentration of 10 μg/ml and the instantaneous capture rate was calculated as a function of time (and also the infused biotinylated Annexin V amount). We found that apoptotic cell capture remained efficient at ~97% when a total of <0.33 μg of biotinylated Annexin V was infused into the device (Fig. 4c). We analyzed a total of ~18,000 cells before the device became saturated with 0.33 μg of biotinylated Annexin V infusion. Beyond this amount, the capture rate was found to steadily decline resulting in only ~3% of cells to be captured after 1.17 μg of biotinylated Annexin V was input. While these measurements clearly showed a capacity limit for our assay due to saturation of avidin-coated surface, 0.33 μg biotinylated Annexin V is enough to analyze ~132K cells, a number that is orders of magnitude larger than the number of cells used for a typical cell viability assay with flow cytometry.

Finally, we studied the effect of flow rate on the cell capture performance (Fig. 4d). The flow rate is a critical parameter for assay - excessively high flow rates can result in false negative results due to inadequate interaction time between biotin-labeled apoptotic cells and the neutravidin-coated chamber surface, while very low flow rates can lead to false positive results due to non-specific binding of non-target cells to the capture chamber. To determine the optimum flow rate, we ran the microchip at different flow rates (50 - 600 μl/hr per inlet) and measured the resulting cell capture efficiency (Fig. 4d). Virtually all (~95%) of the target cells could be captured on the microchip for flow rates <200 μl/hr. At higher flow rates, the capture rate decreased as expected with only ~48% of cells captured at 600 μl/hr. Based on these findings, we set 100 μl/hr (per inlet) as the operational flow rate for the capture chamber. This flow rate allowed for ample avidin-biotin interaction time, facilitating effective capture while minimizing non-specific adhesion artifacts and sedimentation issues that were observed to be prevalent at slower flow rates. All capture rate measurements were conducted within the region

between the entry and exit sensors. We found that the capture rate outside this region, in the fluidic channels on either side of the inlet and outlet sensors, was negligible (<0.5%). This is attributed to the high flow speed of cells within such regions since the channel cross-section is significantly smaller than that of the micropillar-laden capture region. Given the constant volumetric flow rate throughout the device, regions with smaller cross sections experience high flow speeds, resulting in lower capture rate.

Each apoptosis assay we conducted on our microchip-based platform in this work employed a new device for two key reasons: First, at the optimal Annexin V concentration of 10 μg/mL, the capture chamber saturates with unbound Annexin V once it exceeds a threshold amount (> 0.33 μg) infused into the microchip. This necessitates using the microchip for a single run, as its capacity is finite and Annexin V binding in irreversible. Second, our current protocol does not recover the captured cells. Once the capture chamber immobilizes the target cells, it might affect subsequent runs. Our approach of creating disposable devices ensures accurate and reliable assay results by preventing cross-talk between different assays.

3.5.Testing the assay accuracy using control samples

First, we tested the specificity of our optimized assay by processing control samples. Non-apoptotic (n=3) and heat-treated (n=3) apoptotic Jurkat cells were used as negative and positive controls, respectively. Our assay reported an average of ~12.3% of non-apoptotic Jurkat cells to be apoptotic versus ~93.6% of the heat-treated positive control (Fig. 5a). Once we confirmed our assay's ability to discriminate between non-apoptotic and apoptotic cell populations, we processed heterogenous control samples we prepared by mixing untreated and heat-treated cell populations at known ratios (1:1, 1:2, and 2:1) with our device (Fig. 5b). For each mixture processed, our assay determined the mix ratios of non-apoptotic and apoptotic cell subpopulations in close agreement to the nominal ratios used to prepare the samples. These results demonstrated that our assay can quantitatively and accurately report apoptotic cell fraction in a given cell suspension.

Next, we benchmarked our assay against the gold standard assay for cell apoptosis, i.e., flow cytometry-based Annexin V assay. First, we analyzed the untreated and heat-treated Jurkat cell populations using flow cytometry for an independent validation of their apoptotic cell content and confirmed the negative and positive controls we used in our experiments were predominantly composed of non-apoptotic (~93.8%) and apoptotic (~96.4%) cells, respectively (Fig. 5c). Next, we mixed the positive and negative control populations at a 1:1 ratio and processed matches samples using both our assay and a commercial flow cytometer (Materials and methods) (Fig. 5d). Using our microchip, we determined ~48.5% of the mixed cell population was apoptotic, while the flow cytometer reported ~52.2% of the matched population to be apoptotic. In repeated measurements (n=3) on matched samples, we found our assay results to be within <7% of those from flow cytometer. Treating the Annexin V assay run by a flow cytometer as the ground truth, we considered ~7% as the error rate for our assay. This error is likely to be due to several factors. While our microchip-based apoptosis assay and flow cytometry measurements were both based on Annexin V to PS binding, the transduction modalities are vastly different. Greater dynamic range provided by flow cytometer for measuring

surface expression is another factor that might have contributed to differences observed in our results. Having said that, these results demonstrated our microchip-based assay can achieve a level of performance close to a commercial flow cytometer and importantly, with no need for the user to label the sample.

3.6. Serial monitoring of acute T-cell leukemia cell apoptosis

As PS externalization is a time-varying phenomenon, accurately capturing this process throughout its progression would yield valuable insight into the kinetics of apoptosis especially in drug discovery and cell manufacturing applications. To demonstrate the utility of our microchip-based assay for monitoring a cell population as they go through apoptosis, we periodically analyzed samples of a Jurkat cell population briefly (15 mins) exposed to an elevated temperature (70 °C) (Materials and methods) (Fig. 6a). Before heat exposure, only a small fraction (~5.8%) of Jurkat cells were observed to go through apoptosis according to our assay results (Fig. 6a-i). However, at 30 minutes following the heat exposure, the majority cell population was observed to be apoptotic with ~65.9% of the cells expressing PS on their membrane (Fig. 6a-ii). After an hour-long interval in a CO_2 incubator at 37 °C, this time ~88.8% of Jurkat cells were determined to be apoptotic (Fig. 6a-iii). Finally, we analyzed the cells at 6.5 hours after heat exposure and found that virtually all (~97.1%) cells were deemed apoptotic (Fig. 6a-iv).

To independently monitor the apoptosis process, we processed matching samples via Annexin V-based flow cytometry. The flow cytometry results at different time points matched closely with our assay results (Fig. 6b i-iv). While the concordance between our assay and flow cytometry is critical to validate our assay for this longitudinal study, it should be noted that the flow cytometry measurements could only be performed with extensive sample preparation and labeling in contrast with ours that processed cells as sampled. As such, our assay could eventually be used to perform these measurements with higher temporal resolution. Taken together, these from this study demonstrated the potential of our microchip-based assay for longitudinal monitoring of cell populations for apoptosis.

4. DISCUSSION

While we utilized PS expression on cell membrane as biomarkers for apoptosis in this work, PS externalization has also been associated with several other biological events, including cell differentiation, development, signaling, and activation. Therefore, the quantitative detection of PS externalization on a low-cost and portable microchip has the potential to equip scientists with a practical tool to study mechanisms and cellular dynamics underlying various medical conditions such as cancer (Bucur et al., 2012; Carneiro & El-Deiry, 2020; Todaro et al., 2008), inflammation (Huynh et al., 2002; Martin, 2016), immune response (Niehues et al., 2001; Opferman, 2008), and neurodegenerative disorders (Chi et al., 2018; Erekat, 2022; Ma et al., 2022).

Here, we reported an integrated microchip-based assay that automates the Annexin V-based apoptosis assay for detecting programmed cell death by leveraging cell membrane-externalized PS. Benchmarking against the gold standard Annexin V assay using via flow cytometry validated the accuracy of our microchip-based assay with only small discrepancies. These deviations can mainly be attributed to fundamental differences in the sensing modalities. Furthermore, each technique responds differently to the presence of non-target particles, lysed cells and their residues that are produced during preparation, in addition to the inherent impurities within the sample.

Our all-electronic, multistage microfluidic scheme coupled with advanced signal processing and analytics software results in our platform offering distinct advantages over existing alternatives. First, unlike conventional immunocapture-based assays which require the cells in question to be pre-labeled with fluorophore-conjugated probes, our microchip performs all sample manipulation steps within the chip allowing the device to accommodate unlabeled cells. This elimination of the need for sample labeling by the operator not only reduces assay time and prevents sample loss during handling, but also creates the opportunity to run assays on samples where pre-labeling is infeasible or prohibitively challenging.

Second, our microchip transduces bioaffinity-based cell capture events into electrical signals. This capability allows the use of simple electrical hardware to generate the excitation signal and condition the information-bearing signal before it is digitized and processed by software. Notably, high integrated architecture extends the utility of our platform to applications, where minimizing the sample-to-answer time is of high importance. Optical systems, in contrast, involve a combination of complex optical and electrical components. The integrated nature of our system makes it viable in a wider range of settings than its more complex counterparts.

Third, the incorporation of a biochemical assay with an electronic sensing scheme allowed us to create a microchip that leverages the advantages of both detection modalities. In contrast to other electronic assays that rely on indirect cytometry via size and electrical properties of the cells within the sample, our approach directly interacts with the cell membrane antigens, utilizing the well-established biochemical markers to perform the measurement. This advancement not only enhances the platform's compatibility and reliability with existing apoptosis assay techniques but also ensures a heightened level of accuracy and specificity in the analysis.

Lastly, our microchip stands out for its affordability and versatility. Unlike traditional assays that require expensive and bulky systems such as flow cytometers, our microchip-based apoptosis assay provides a more cost-effective solution. Each microchip uses inexpensive surface modification reagents, costing less than $5 per chip in research settings, and can be easily reconfigured for different assays and cell types. This flexibility extends to scalable cell processing, as the device’s design and surface area can be adjusted to meet diverse bioanalytical needs. The device is intentionally designed for single use to minimize contamination risks, a crucial consideration in clinical point-of-care settings. Moreover, its portable form factor allows for on-demand assays, making critical testing possible outside of centralized laboratories. The all-electronic, label-free analysis ensures both convenience and reliability, making the microchip suitable for a wide range of scenarios and applications.

5. CONCLUSION

We have developed a microchip-based apoptosis assay that combines the specificity of biochemical assays with the practicality of electronic devices for data acquisition and transmission. Furthermore, the assay does not require sample labeling setting it apart from the conventional biochemical apoptosis assays. Given the cell viability is a widely employed endpoint in a variety of studies, an electronic device that can automatically quantify apoptotic cell population in a sample and achieve this with a specificity and sensitivity comparable to existing labor- and capital-intensive workflows could revolutionize variety of fields including basic cell and immunology research, drug discovery and cell manufacturing.

CRediT AUTHORSHIP CONTRIBUTION STATEMENT

A K M Arifuzzman: Conceptualization, Methodology, Investigation, Validation, Writing – original draft, Writing – review & editing. **Norh Asmare:** Software, Investigation, Writing – original draft, review & editing. **Tevhide Ozkaya-Ahmadov:** Resources. **Aref Valipour:** Resources. **A. Fatih Sarioglu:** Conceptualization, Methodology, Supervision, Writing, – original draft, Writing – review & editing, Funding acquisition.

DECLARATION OF COMPETING INTEREST

The authors declare that they have no known competing financial interests or personal relationships that could have appeared to influence the work reported in this paper.

ACKNOWLEDGEMENTS

This work was supported by the Arnold and Mabel Beckman Foundation, USA (Beckman Young Investigator Award to A.F.S.) and the National Science Foundation, USA (Award No. ECCS 1752170).

REFERENCES

Abbady, A. Q., Twair, A., Ali, B., & Murad, H. (2017). Characterization of annexin V fusion with the superfolder GFP in liposomes binding and apoptosis detection. *Frontiers in Physiology*, 8.

Arifuzzman, A. K. M., Asmare, N., Ozkaya-Ahmadov, T., Civelekoglu, O., Wang, N., & Sarioglu, A. F. (2023). An autonomous microchip for real-time, label-free immune cell analysis. *Biosensors and Bioelectronics*, 222.

Balasubramanian, K., Mirnikjoo, B., & Schroit, A. J. (2007). Regulated externalization of phosphatidylserine at the cell surface: Implications for apoptosis. *Journal of Biological Chemistry*, 282(25), 18357–18364.

Bucur, O., Stancu, A. L., Khosravi-Far, R., & Almasan, A. (2012). Analysis of apoptosis methods recently used in Cancer Research and Cell Death &disease publications. *Cell Death and Disease,* 3(2).

Carneiro, B. A., & El-Deiry, W. S. (2020). Targeting apoptosis in cancer therapy. *Nature Reviews Clinical Oncology*, 17(7), 395–417.

Chen, H., Zhang, J., Gao, Y., Liu, S., Koh, K., Zhu, X., & Yin, Y. (2015). Sensitive cell apoptosis assay based on caspase-3 activity detection with graphene oxide-assisted electrochemical signal amplification. *Biosensors and Bioelectronics*, 68, 777–782.

Chi, H., Chang, H. Y., & Sang, T. K. (2018). Neuronal cell death mechanisms in major neurodegenerative diseases. *International Journal of Molecular Sciences*, 19(10).

Chong, L. H., Ching, T., Farm, H. J., Grenci, G., Chiam, K. H., & Toh, Y. C. (2022). Integration of a microfluidic multicellular coculture array with machine learning analysis to predict adverse cutaneous drug reactions. *Lab on a Chip,* 22(10), 1890-1904.

Civelekoglu, O., Liu, R., Usanmaz, C. F., Chu, C. H., Boya, M., Ozkaya-Ahmadov, T., Arifuzzman, A. K. M., Wang, N., & Sarioglu, A. F. (2022). Electronic measurement of cell antigen expression in whole blood. *Lab on a Chip*, 22(2), 296–312.

Civelekoglu, O., Ozkaya-Ahmadov, T., Arifuzzman, A. K. M., Islak Mutcali, S., & Sarioglu, A. F. (2022). Immunomagnetic leukocyte differential in whole blood on an electronic microdevice. *Lab on a Chip*, 22(12), 2331–2342.

Civelekoglu, O., Wang, N., Arifuzzman, A. K. M., Boya, M., & Sarioglu, A. F. (2022). Automated lightless cytometry on a microchip with adaptive immunomagnetic manipulation. *Biosensors and Bioelectronics*, 203.

Civelekoglu, O., Wang, N., Boya, M., Ozkaya-Ahmadov, T., Liu, R., & Sarioglu, A. F. (2019). Electronic profiling of membrane antigen expression via immunomagnetic cell manipulation. *Lab on a Chip*, 19(14), 2444–2455.

D'Arcy, M. S. (2019). Cell death: a review of the major forms of apoptosis, necrosis and autophagy. *Cell Biology International,* 43(6), 582–592.

Darzynkiewicz, Z., Huang, X., Okafuji, M., & King, M. A. (2004). Cytometric Methods to Detect Apoptosis. *Methods in Cell Biolog*y, 75, 307-341.

Dong, C., Song, C., Chao, J., Xiong, J., Fang, X., Zhang, J., Zhu, Y., Zhang, Y., & Wang, L. (2022). Multi-armed tetrahedral DNA probes for visualizing the whole-course of cell apoptosis by simultaneously fluorescence imaging intracellular cytochrome c and telomerase. *Biosensors and Bioelectronics*, 205.

Erekat, N. S. (2022). Apoptosis and its therapeutic implications in neurodegenerative diseases. In *Clinical Anatomy,* 35(1), 65–78.

Fischer, K., Andreesen, R., & Mackensen, A. (2002). An improved flow cytometric assay for the determination of cytotoxic T lymphocyte activity. *Journal of Immunological Methods,* 259(1-2), 159-169.

Galluzzi, L., Vitale, I., Aaronson, S. A., Abrams, J. M., Adam, D., Agostinis, P., Alnemri, E. S., Altucci, L., Amelio, I., Andrews, D. W., Annicchiarico-Petruzzelli, M., Antonov, A. V., Arama, E., Baehrecke, E. H., Barlev, N. A., Bazan, N. G., Bernassola, F., Bertrand, M. J. M., Bianchi, K., … Kroemer, G. (2018). Molecular mechanisms of cell death: Recommendations of the Nomenclature Committee on Cell Death 2018. *Cell Death and Differentiation*, 25(3), 486–541.

Huynh, M.-L. N., Fadok, V. A., & Henson, P. M. (2002). Phosphatidylserine-dependent ingestion of apoptotic cells promotes TGF-β1 secretion and the resolution of inflammation. *Journal of Clinical Investigation*, 109(1), 41–50.

Kerr, J. F. R., Wyllie, A. H., & Currie, A. R. (1972). Apoptosis: a basic biological phenomenon with wide-ranging implications in tissue kinetics. *British Journal of Cancer*, 26(4), 239-257.

Kopeina, G. S., & Zhivotovsky, B. (2022). Programmed cell death: Past, present and future. *Biochemical and Biophysical Research Communications*, 633, 55–58.

Koskinen, J. O., Vaarno, J., Meltola, N. J., Soini, J. T., Hänninen, P. E., Luotola, J., Waris, M. E., & Soini, A. E. (2004). Fluorescent nanoparticles as labels for immunometric assay of C-reactive protein using two-photon excitation assay technology. *Analytical Biochemistry*, 328(2), 210–218.

Leber, B., Mayrhauser, U., Leopold, B., Koestenbauer, S., Tscheliessnigg, K., Stadlbauer, V., & Stiegler, P. (2012). Impact of Temperature on Cell Death in a Cell-culture Model of Hepatocellular Carcinoma. *Anticancer Research*, 32(3), 915–922.

Liu, R., Arifuzzman, A. K. M., Wang, N., Civelekoglu, O., & Sarioglu, A. F. (2020). Electronic Immunoaffinity Assay for Differential Leukocyte Counts. *Journal of Microelectromechanical Systems*, 29(5), 942–947.

Liu, R., Chu, C. H., Wang, N., Ozkaya-Ahmadov, T., Civelekoglu, O., Lee, D., Arifuzzman, A. K. M., & Sarioglu, A. F. (2019). Combinatorial Immunophenotyping of Cell Populations with an Electronic Antibody Microarray. *Small*, 15(51).

Liu, R., Waheed, W., Wang, N., Civelekoglu, O., Boya, M., Chu, C. H., & Sarioglu, A. F. (2017). Design and modeling of electrode networks for code-division multiplexed resistive pulse sensing in microfluidic devices. *Lab on a Chip*, 17(15), 2650–2666.

Liu, R., Wang, N., Kamili, F., & Sarioglu, A. F. (2016). Microfluidic CODES: A scalable multiplexed electronic sensor for orthogonal detection of particles in microfluidic channels. *Lab on a Chip*, *16*(8), 1350–1357.

Ma, X., Li, X., Wang, W., Zhang, M., Yang, B., & Miao, Z. (2022). Phosphatidylserine, inflammation, and central nervous system diseases. *Frontiers in Aging Neuroscience*, 14.

Martin, S. J. (2016). Cell death and inflammation: the case for IL-1 family cytokines as the canonical DAMPs of the immune system. *FEBS Journal*, 283(14), 2599–2615.

Meers, P., & Mealy, T. (1993). Calcium-Dependent Annexin V Binding to Phospholipids: Stoichiometry, Specificity, and the Role of Negative Charge. *Biochemistry*, 32(43), 11711-11721.

Niehues, T., McCloskey, T. W., Ndagijimana, J., Horneff, G., Wahn, V., & Pahwa, S. (2001). Apoptosis in T-lymphocyte subsets in human immunodeficiency virus-infected children measured immediately ex vivo and following in vitro activation. *Clinical and Diagnostic Laboratory Immunology*, 8(1), 74–78.

Opferman, J. T. (2008). Apoptosis in the development of the immune system. In *Cell Death and Differentiation*, 15(2), 234–242.

São Pedro, M. N., Santos, M. S., Eppink, M. H. M., & Ottens, M. (2023). Design of a microfluidic mixer channel: First steps into creating a fluorescent dye-based biosensor for mAb aggregate detection. *Biotechnology Journal*, *18*(1).

Schutte, B., Nuydens, R., Geerts, H., & Ramaekers, F. (1998). Annexin V binding assay as a tool to measure apoptosis in differentiated neuronal cells. *Journal of Neuroscience Methods,* 86(1), 63-69.

Taylor, R. C., Cullen, S. P., & Martin, S. J. (2008). Apoptosis: Controlled demolition at the cellular level. *Nature Reviews Molecular Cell Biology*, 9(3), 231–241.

Todaro, M., Lombardo, Y., Francipane, M. G., Perez Alea, M., Cammareri, P., Iovino, F., Di Stefano, A. B., Di Bernardo, C., Agrusa, A., Condorelli, G., Walczak, H., & Stassi, G. (2008). Apoptosis resistance in epithelial tumors is mediated by tumor-cell-derived interleukin-4. *Cell Death and Differentiation*, *15*(4), 762–772.

Tong, C., Shi, B., Xiao, X., Liao, H., Zheng, Y., Shen, G., Tang, D., & Liu, X. (2009). An Annexin V-based biosensor for quantitatively detecting early apoptotic cells. *Biosensors and Bioelectronics*, *24*(6), 1777–1782.

Vermes, I., Haanen, C., Steffens-Nakken, H., & Reutelingsperger, C. (1995). A novel assay for apoptosis Flow cytometric detection of phosphatidylserine early apoptotic cells using fluorescein labelled expression on Annexin V. *Journal of Immunological Methods*, 184(1), 39-51.

Vermette, P., Gengenbach, T., Divisekera, U., Kambouris, P. A., Griesser, H. J., & Meagher, L. (2003). Immobilization and surface characterization of NeutrAvidin biotin-binding protein on different hydrogel interlayers. *Journal of Colloid and Interface Science*, *259*(1), 13–26.

Worsley, C. M., Veale, R. B., & Mayne, E. S. (2022). Inducing apoptosis using chemical treatment and acidic pH, and detecting it using the Annexin V flow cytometric assay. *PLoS ONE*, *17*(6).

1 **Figures**

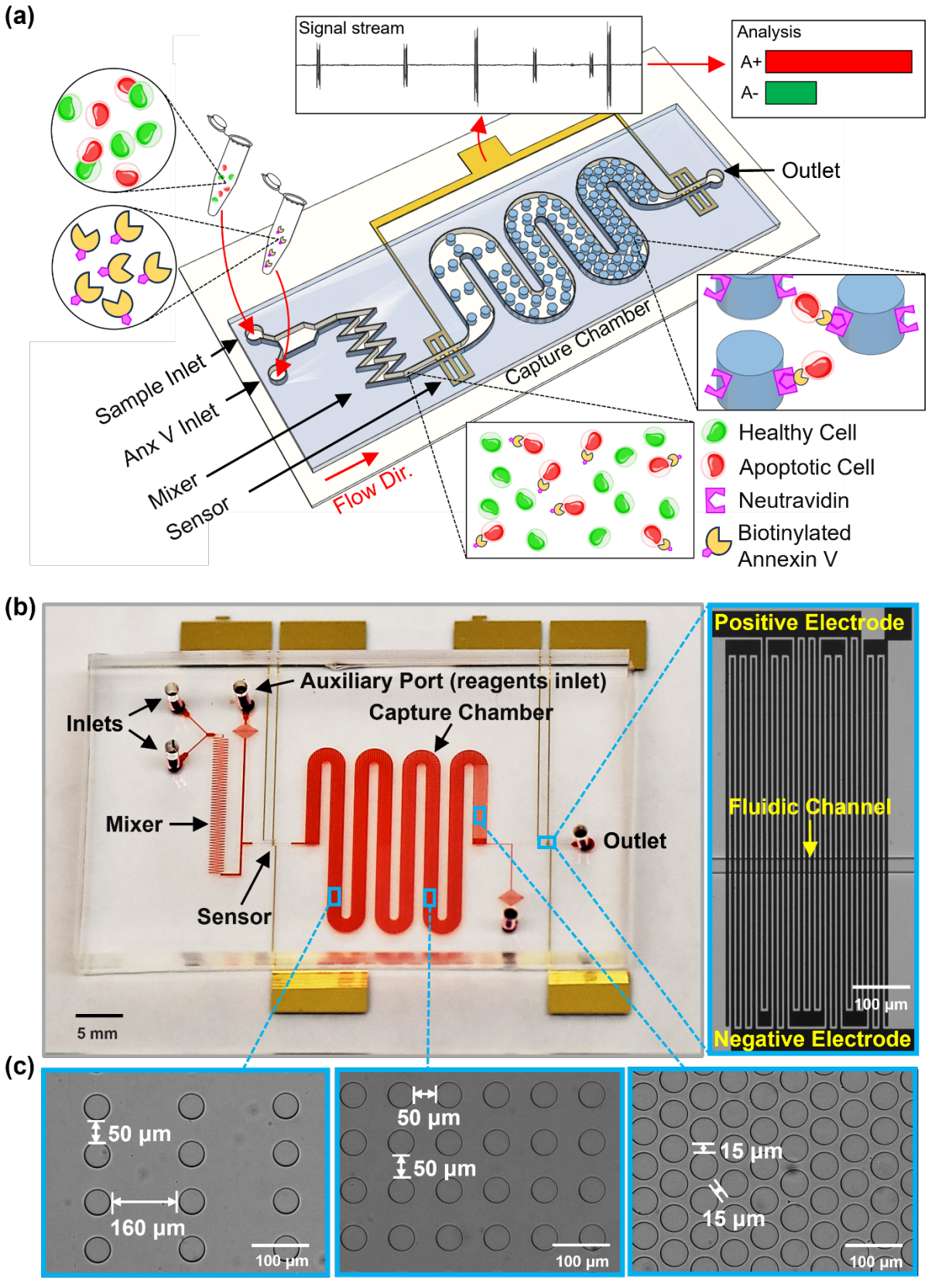
(a)
Signal stream
Analysis
A+
A-
Outlet
Sample Inlet
Anx V Inlet
Mixer
Sensor
Flow Dir.
Capture Chamber
Healthy Cell
Apoptotic Cell
Neutravidin
Biotinylated Annexin V
(b)
Auxiliary Port (reagents inlet)
Capture Chamber
Inlets
Mixer
Outlet
Sensor
5 mm
Positive Electrode
Fluidic Channel
100 µm
Negative Electrode
(c)
50 µm
160 µm
100 µm
50 µm
50 µm
100 µm
15 µm
15 µm
100 µm

2

Fig. 1: Workflow and microchip design for microchip-based apoptosis assay. (a) A schematic representation of the microchip-based apoptosis assay. The microchip automatically labels the cell population with Annexin V solution through a built-in micromixer and subsequently captures apoptotic cells that have underwent PS externalization in a functionalized chamber. An integrated barcoded sensor network transduces apoptotic cell capture events into an electrical signal, which is subsequently processed to compute the fraction of apoptotic cells in a sample. (b) A photograph of the fabricated microchip, whose microchannels were filled with a red dye for visualization purposes. Au electrode traces forming the on-chip electrical sensor network can also be seen sandwiched between the microfluidic channels and the glass substrate. Insets show close-up microscope images of the coded electrical sensors on the device, along with the microfluidic channels they monitor. (c) Microscope images of the micropillars and their spacing at the three different zones of the capture chamber, which maximizes interaction with cells as they flow through the device.

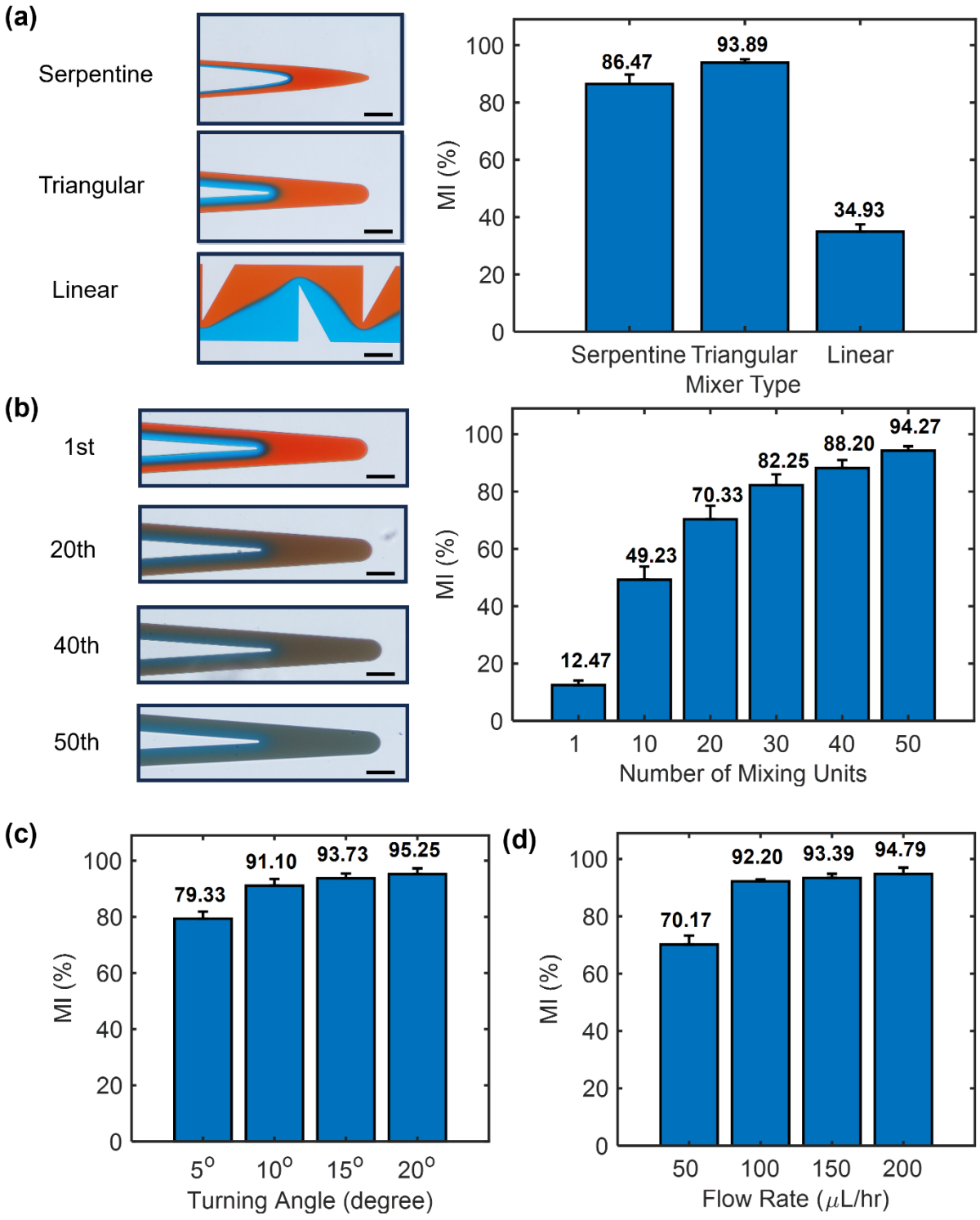

Fig. 2. Characterization of the on-chip micromixer. (a) (Left) The bright field microscope images showing single mixing units of three different micromixer designs investigated in this study. (Right) Measured mixing performance for the three micromixer designs each comprising of 50 mixing units and driven at 100 μL/hr from both inlets. (b) (Left) Colored microscope images of the triangular mixer in operation taken at different positions. The images show increasingly

mixed colors further along the micromixer. (Right) A plot showing the calculated MI values based on the color measurements taken at different points along the micromixer when driven at 100 μL/hr from both inlets. (c) A plot of calculated MI values for different micromixers designed to have different turn angles (5^o, 10^o, 15^o, and 20^o). The measurements were taken at the outlets of the micromixer designed with 50 mixing units, using a flow rate of 100 μL/hr at both inlets. (d) Characterization of the optimized micromixer as a function of the flow rate. The plot shows the MI values calculated based on the measurements taken at the outlet of the micromixer. For all bar plots, the bar heights and error bars represent the mean (n=3) and standard error, respectively. Scale bars, 100 μm.

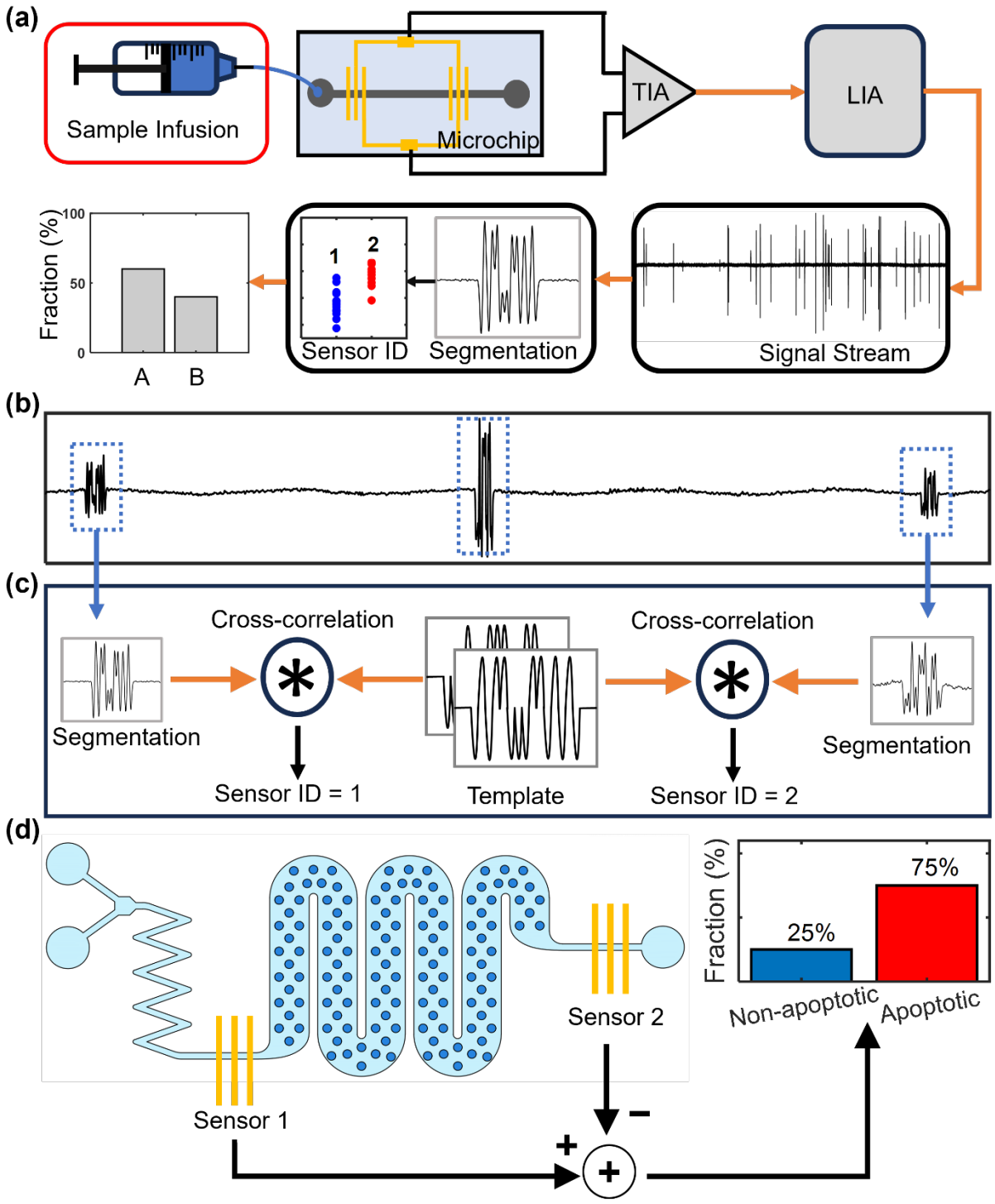
(a)
Sample Infusion
Microchip
TIA
LIA
Fraction (%)
100
50
0
A
B
1
2
Sensor ID
Segmentation
Signal Stream
(b)
(c)
Cross-correlation
Cross-correlation
Segmentation
Segmentation
Sensor ID = 1
Template
Sensor ID = 2
(d)
Sensor 2
Sensor 1
Fraction (%)
25%
75%
Non-apoptotic
Apoptotic

1

2

3

4

Fig. 3. Processing of electrical data from the developed apoptosis assay. (a) A schematic showing the individual steps in the operation of the developed microchip-based apoptosis assay system. (b) A representative section of the recorded signal stream after it was demodulated by the LIA. (c) A schematic representation of steps used in signal classification process. Waveforms from sensors are correlated with a pre-assembled template library for identification. (d) A schematic depicting how sensor signals were used to derive the number of captured cells (i.e., the apoptotic cells).

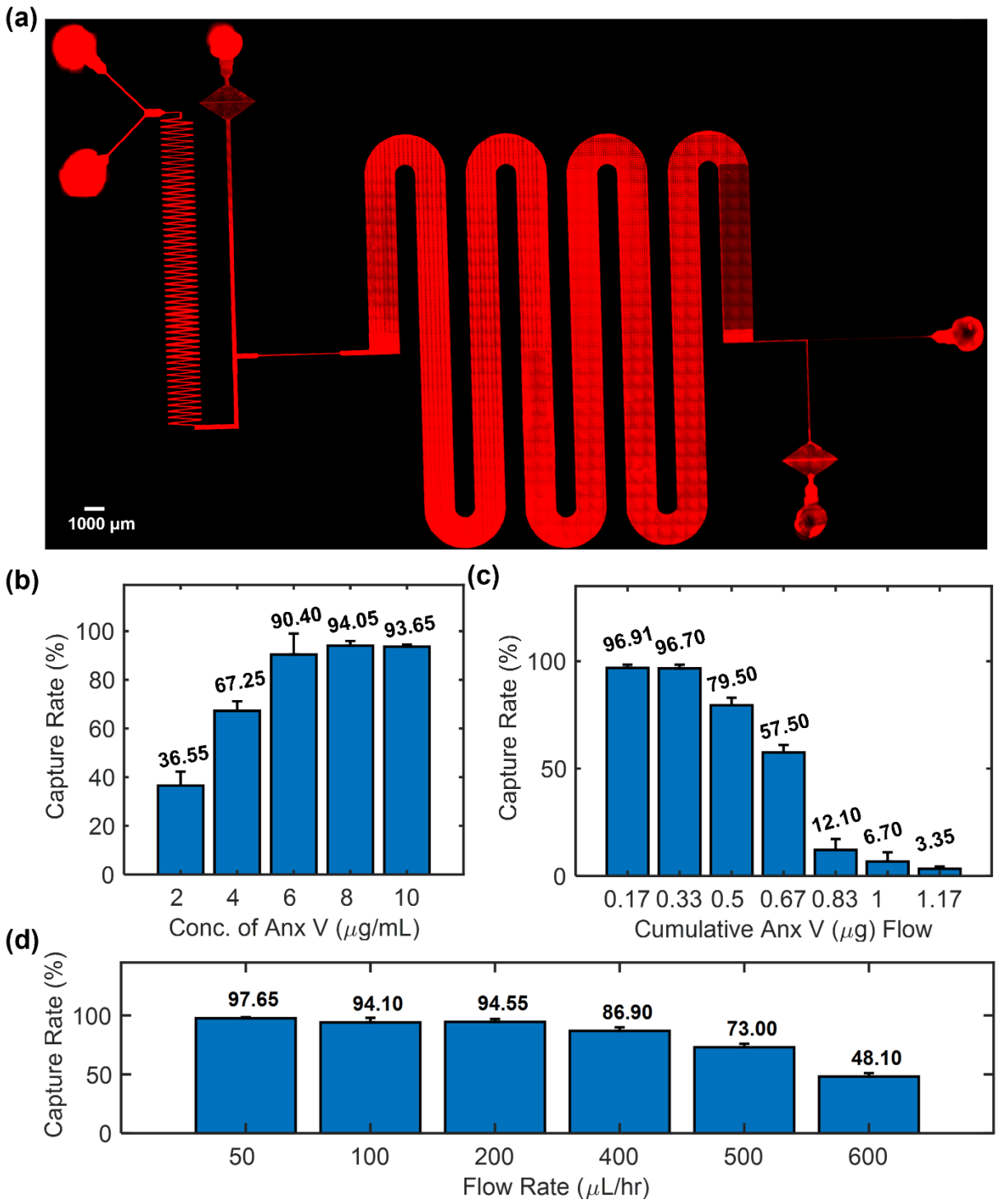
(a)
1000 µm
(b)
Capture Rate (%)
0
20
40
60
80
100
36.55
67.25
90.40
94.05
93.65
2
4
6
8
10
Conc. of Anx V (µg/mL)
(c)
Capture Rate (%)
0
50
100
96.91
96.70
79.50
57.50
12.10
6.70
3.35
0.17
0.33
0.5
0.67
0.83
1
1.17
Cumulative Anx V (µg) Flow
(d)
Capture Rate (%)
0
50
100
97.65
94.10
94.55
86.90
73.00
48.10
50
100
200
400
500
600
Flow Rate (µL/hr)

1

2

3

4

Fig. 4. Optimization of the assay for apoptotic cell capture. (a) A fluorescence microscopy image of the microchip functionalized with neutravidin. Cy5 fluorophore-conjugated biotin molecules captured by the neutravidin-coated surface confirms the chemically active device surface. (b) A plot showing the apoptotic cell capture rates measured for varying concentrations of biotinylated Annexin V in the on-chip labeling solution. (c) Instantaneous apoptotic cell capture rate measured as the unbound biotinylated Annexin V accumulated on the inner surfaces of the microchip, whose functionalized surface was eventually neutralized leading to diminished cell capture rates. (d) Capture rates of the optimized assay measured for different sample flow rates. For all bar plots, the bar heights and error bars represent the mean (n=3) and standard error, respectively.

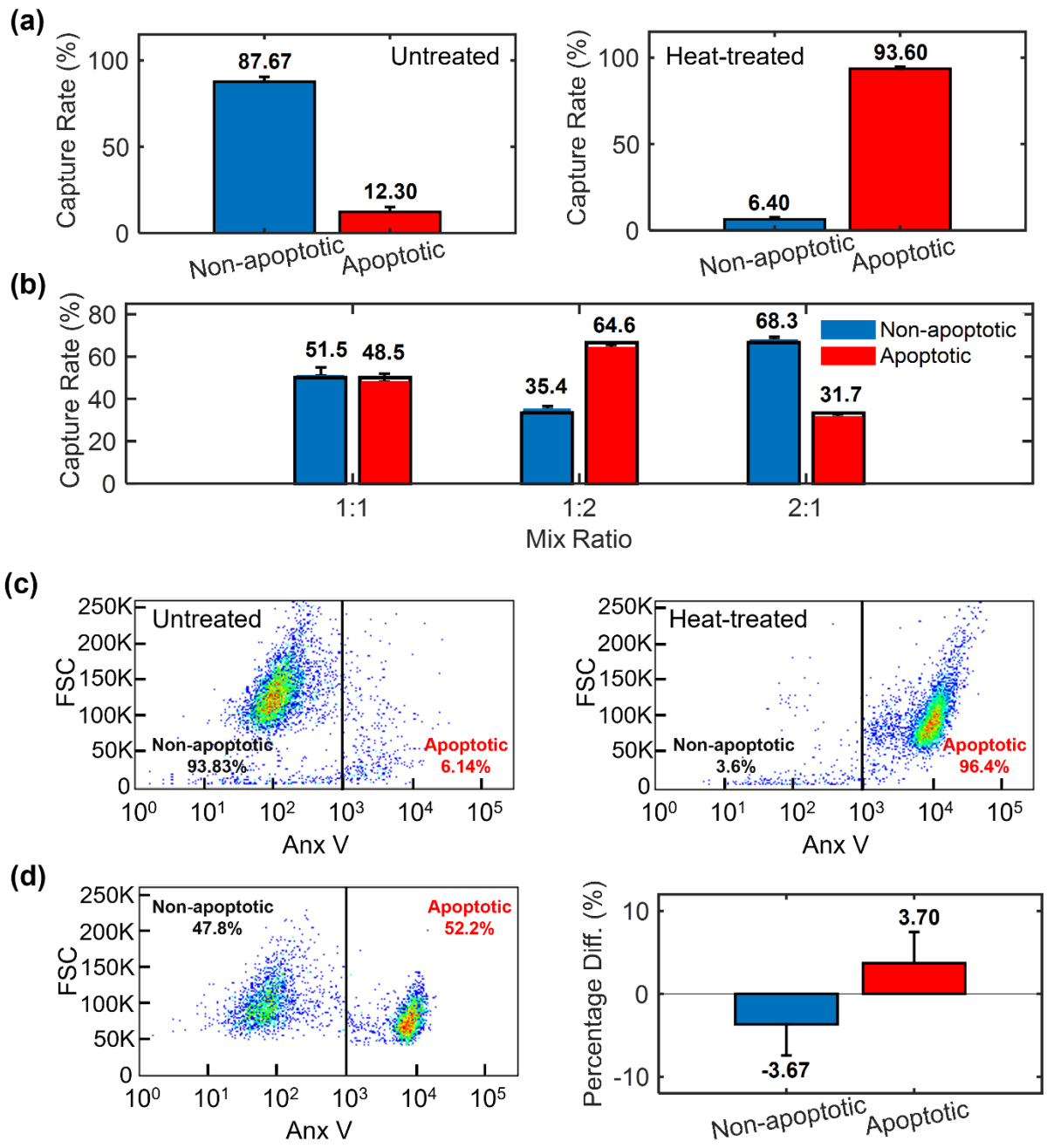

Fig. 5. Evaluating the accuracy of our assay using control samples (a) Counts of non-apoptotic and apoptotic cells determined by our assay for untreated (left) and heat-treated (right) Jurkat cell population. (b) The figure shows the frequencies of non-apoptotic and apoptotic Jurkat cell subpopulations as measured by our system (colored bars) compared to the nominal mix ratios (1:1, 1:2, and 2:1) determined by a hemocytometer (unfilled bars). The agreement between our results and the nominal mixing ratios validates the assay accuracy. (c) Plots of PS expression of untreated (left) and heat-treated (right) Jurkat cell controls measured with through flow cytometry via Annexin V labeling. Cells were gated based on PS expression and were scored as either non-apoptotic or apoptotic (d) (Left) The plot illustrates PS expression measured in a

sample containing a 1:1 mix of non-apoptotic and apoptotic Jurkat cells using flow cytometry. Non-apoptotic and apoptotic cells were gated based on PS expression. (Right) The figure shows the differences in the measured non-apoptotic and apoptotic cell fractions in matched samples between flow cytometry and our microchip-based apoptosis assay. The flow cytometer results were taken as the reference. For all bar plots, the bar heights and error bars represent the mean (n=3) and standard error, respectively.

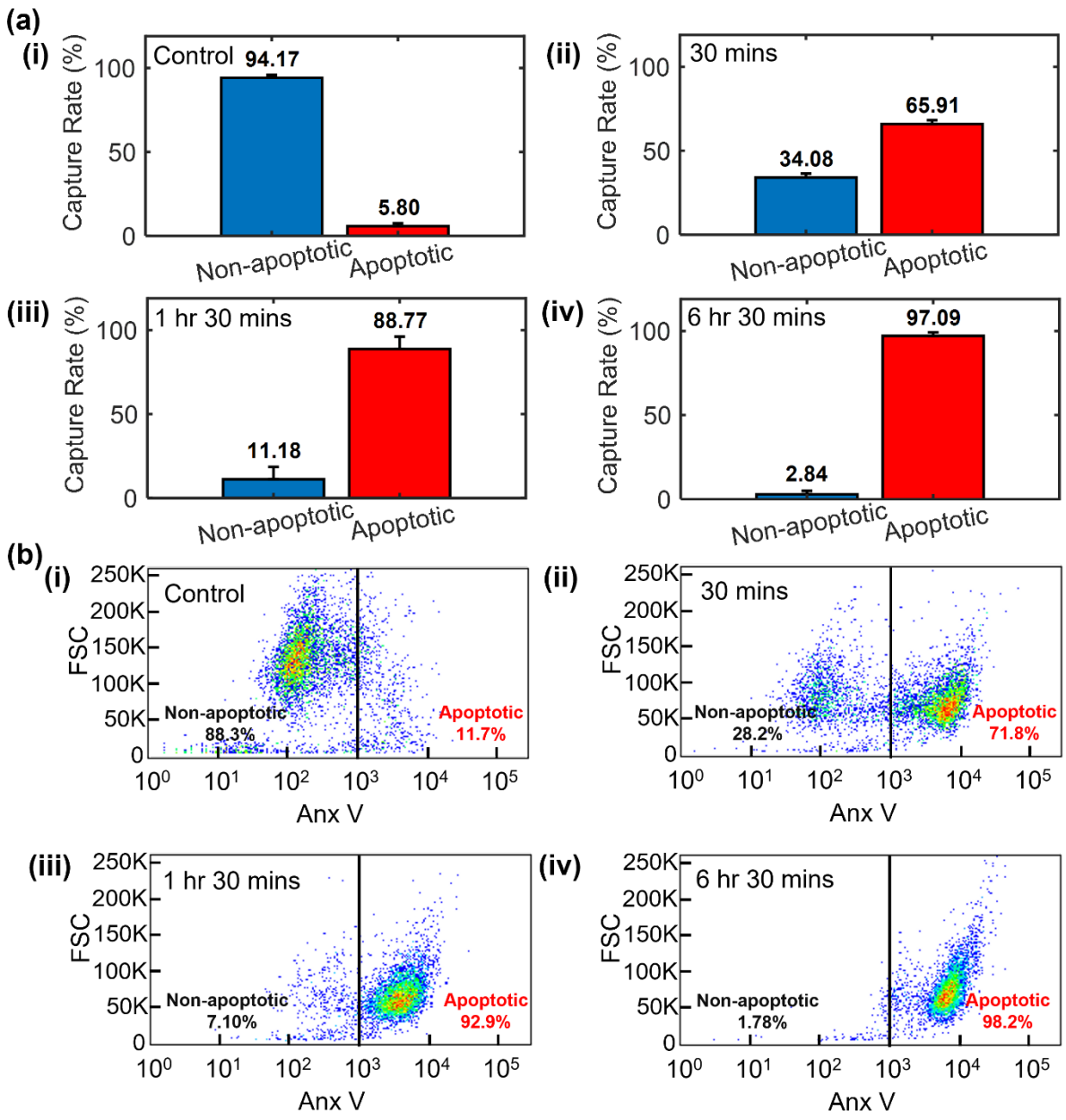

Fig. 6. Serial monitoring of acute T-cell leukemia cell apoptosis. (a) Sequential measurement of PS externalization in Jurkat cells using our microchip-based apoptosis assay. The measurements were done (i) before any heat exposure and at (ii) 30 minutes, (iii) 1.5 hours, and (iv) 6.5 hours after the heat exposure. For all bar plots, the bar heights and error bars represent the mean (n=3) and standard error, respectively. (b) Plots show the PS expression measured in samples matched to those analyzed in (a) via flow cytometry for validation of our assay results.

SUPPLEMENTARY INFORMATION

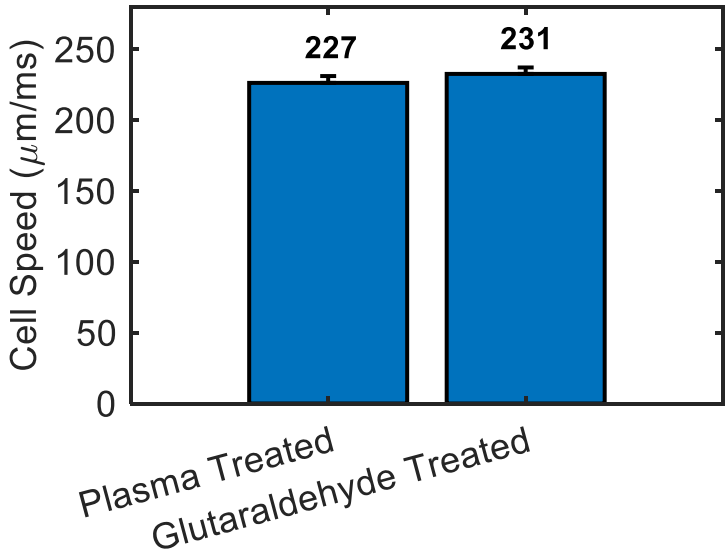

Fig. S1. Comparison of cell speed within plasma treated microchips with and without glutaraldehyde treatment. The samples were infused into the microchip using a syringe pump at a flow rate of 100 µL/hr. The cell speed was measured within the microfluidic channel, which has dimensions of 20 µm in width and 20 µm in height. High speed camera footage (10,000 fps) was captured for both devices, and the field of view was placed at identical locations in both cases. An image processing program was developed to track each cell as it traversed the channel. The footage was denoised, background subtracted to isolate the movement of the cells within the frame and processed through a tracker that followed any visible cells throughout their time within the camera's view. To minimize error from any minute, irregular flow behavior of the cells, all the translations they made were collected over multiple frames (≥ 10) before being averaged. This was done for all cells and repeated for both devices. The comparison shows there is no appreciable effect of glutaraldehyde treatment on cell flow speed within the microfluidic channel.

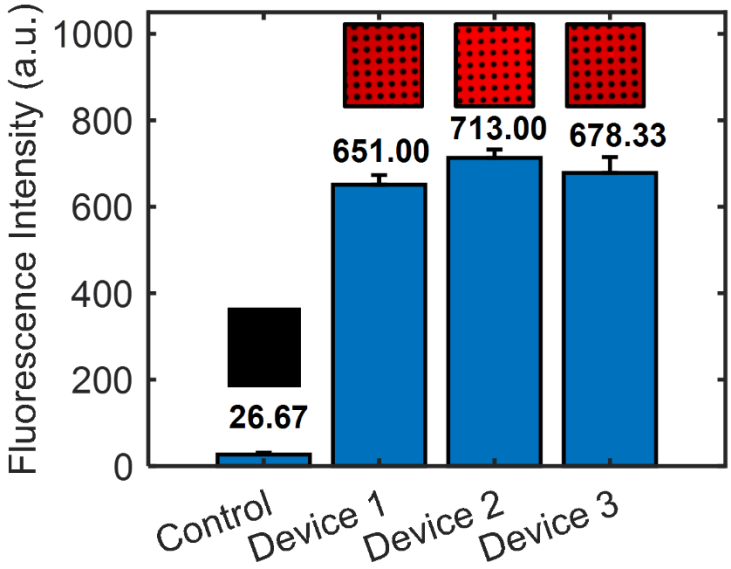

Fig. S2. Comparison of fluorescence intensity across four identical devices. Three devices were functionalized with the same amount of neutravidin (166.7 µg), while the control device remained untreated. Each device was then incubated with Cy5 biotin. Fluorescence intensity measurements were taken at three different locations on each device using a fluorescence microscope. The average peak fluorescence intensity for each device was then calculated based on these three measurements. Insets show fluorescence images of the capture chambers from each device captured using a fluorescence microscope. The similarity found between the average fluorescence intensities across the three neutravidin-functionalized devices confirms that Cy5 biotin was conjugated to the immobilized neutravidin in a reproducible manner, thus validating the consistency of our functionalization process.

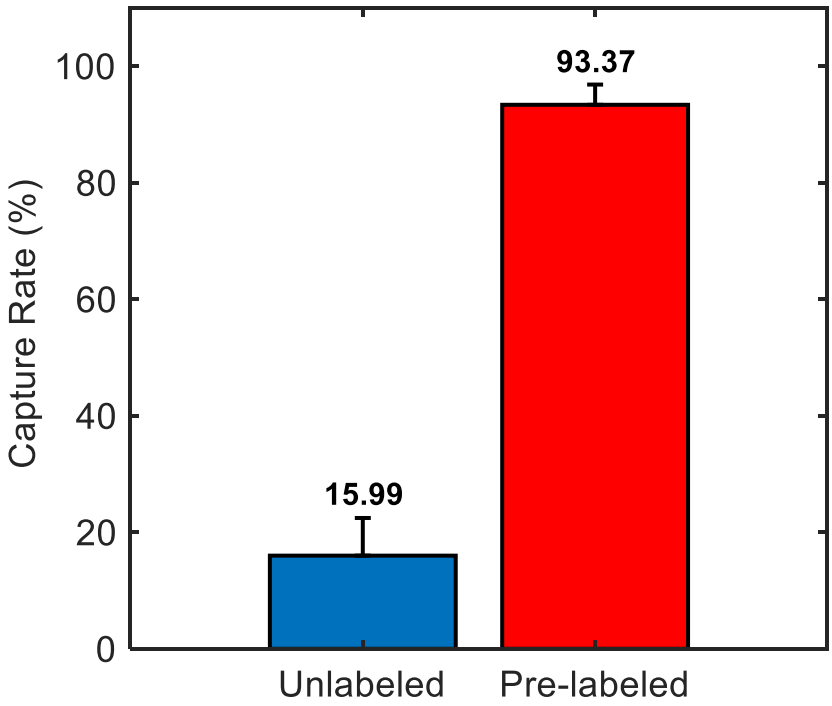

Fig. S3. The effect of pre-labeling of apoptotic cells on capture efficiency. The plot shows the measured rates of capture of apoptotic cells with Annexin V-PS and avidin-biotin binding. To utilize stronger avidin-biotin binding, cells were pre-labeled with biotinylated Annexin V and then captured on neutravidin-coated surfaces. For this plot, the bar heights and error bars represent the mean (n=3) and standard error, respectively.

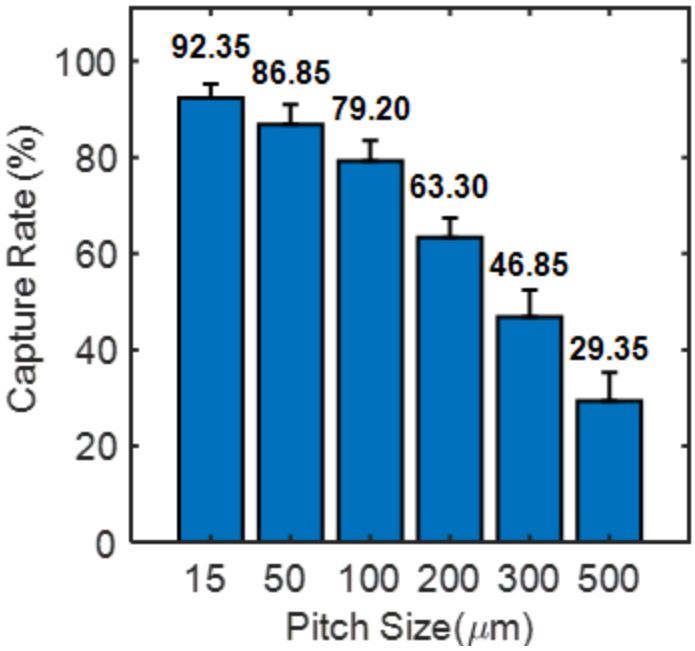

Fig. S4. The plot illustrates the impact of micropillar density on the capture efficiency of apoptotic cells. It displays the measured capture rates of apoptotic cells with grid patterned pitch sizes ranging from 15 µm to 500 µm. Shorter pitch micropillars in the capture chamber result in higher capture efficiency due to increased interaction between the cells and the neutravidin-coated pillars. In contrast, longer pitch micropillars lead to a lower capture rate, approximately 29%. In this plot, the bar heights and error bars represent the mean (n=3) and standard error, respectively.

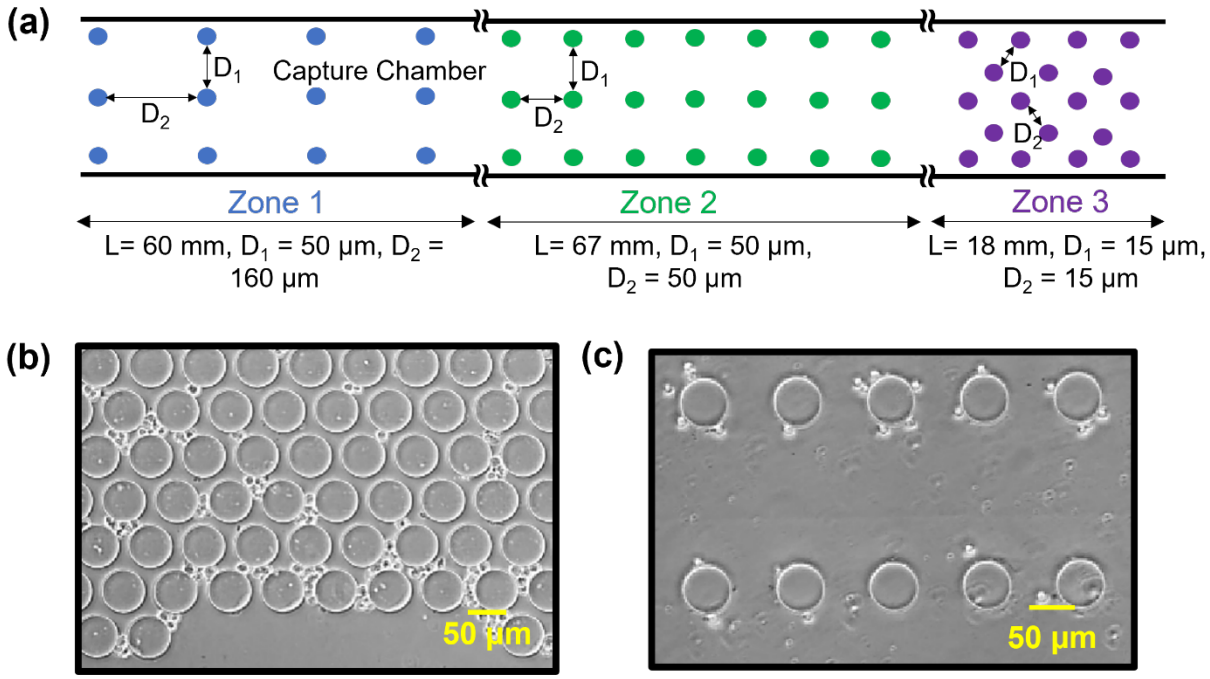

Fig. S5. Pillar Density Arrangement in the Device. (a) The device is segmented into three zones with varying densities of pillars (pillar diameter 60 µm). Zone 1 (length, L = 60 mm) features a lower density to prevent upstream cell clogging and unintended cell capture. Pillar density gradually increases in Zone 2 (length, L = 67 mm) to enhance capture efficiency, while Zone 3 (length, L = 18 mm) has the highest density to maximize the capture rate. (b) Initial high-density pillars at the onset of the capture chamber led to cell clogging and mechanical cell trapping, resulting in false-positive cell capture. (c) Lower density pillars in Zone 1 effectively mitigate cell clogging, ensuring accurate cell capture.

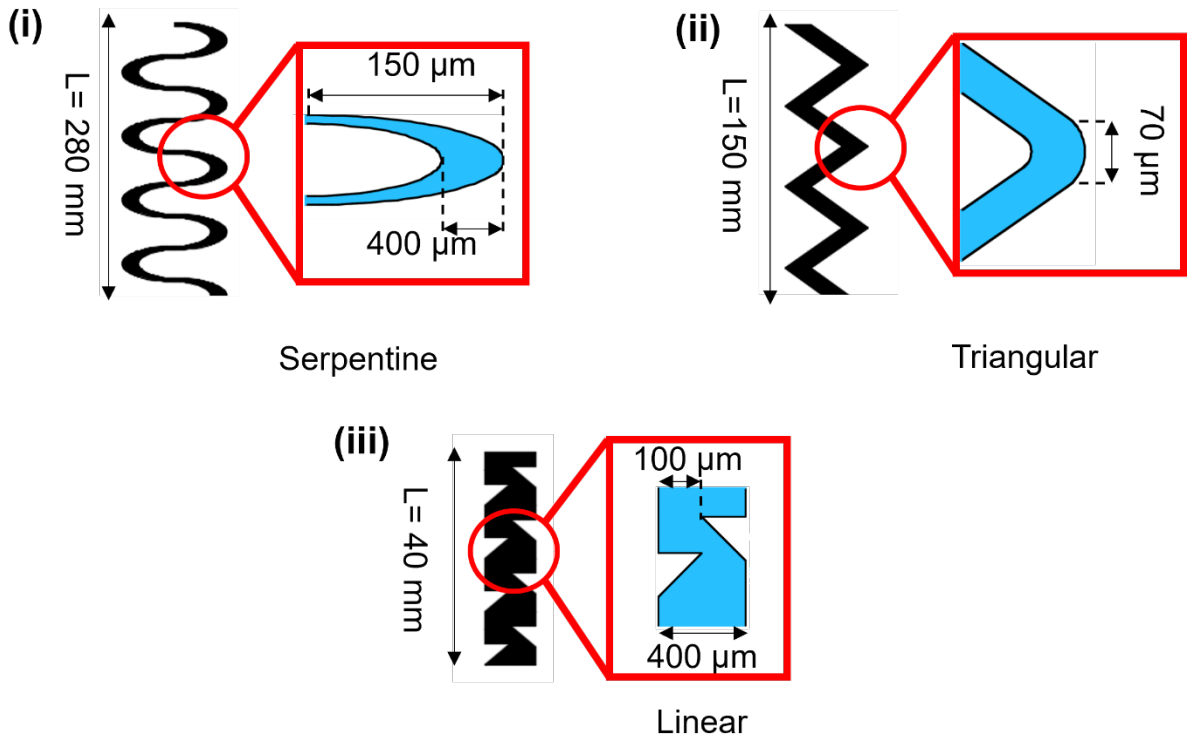

Fig. S6. Schematic drawings showing different micromixer geometries investigated for this study, namely (i) a serpentine micromixer with a total mixing length of 280 mm, (ii) a triangular micromixer with a total mixing length of 150 mm and (iii) a linear micromixer with a total mixing length of 40 mm. Each micromixer tested comprised 50 of the mixing units shown in close-up.